Journal of Membrane Science 428 (2013) 410–424

Contents lists available at SciVerse ScienceDirect

Journal of Membrane Science

journal homepage: www.elsevier.com/locate/memsci

A two-interface transport model with pore-size distribution for predicting the performance of direct contact membrane distillation (DCMD)

Albert S. Kim [a,b,*]

[a] Department of Civil and Environmental Engineering, University of Hawaii at Manoa, 2540 Dole Street, Honolulu, HI 96822, USA
[b] Department of Chemical Engineering, College of Engineering, Kyung Hee University, Gyeonggi-do 446-701, Korea

ARTICLE INFO

Article history:
Received 9 August 2012
Received in revised form
29 September 2012
Accepted 6 October 2012
Available online 6 November 2012

Keywords:
Direct contact membrane distillation
Clausius–Clapeyron equation
Bosanquet relation
Mean free path

ABSTRACT

We investigated fundamental aspects of heat and mass transfer of direct contact membrane distillation. Molar flux of water vapor through a membrane pore was analytically obtained by solving Fick's law in the original differential form. Axial variation of the temperature profile was derived as exponentially decreasing, and was found to be linear due to small membrane thickness and dominant heat conduction through the solid part of the membrane. An alternative expression of water vapor pressure at a constant temperature was developed using experimental data of water latent heat for evaporation, and was used to calculate the concentration of water vapor in the membrane pore. The effective diffusion coefficient was obtained by combining Knudsen and Brownian diffusion coefficients with Bosanquet's assumption. The effective diffusivity and mean free path of water vapor slowly decrease in the axial direction, and the vapor concentration increases along the membrane pore primarily due to the linearly decreasing temperature. We found that the required heat flux monotonously increases with the vapor flux through membrane pores. Finite variance of a pore size distribution provides less vapor flux than that of mono-dispersed pores. This is because a number of smaller pores than the average pore size significantly hinders the vapor transport across the porous membrane. Theoretical prediction of permeate flux agrees very well with experimental observations reported in the literature.

© 2012 Elsevier B.V. All rights reserved.

1. Introduction

Direct contact membrane distillation (DCMD) is one type of membrane distillation (MD) process in which both the liquid feed and liquid permeate are kept in contact with the membrane interface [1,2]. Feed solution containing various solute species is maintained at a higher temperature (50–70 °C) than that of the permeate stream of cold freshwater (10–25 °C). The temperature difference between the two solutions generates a partial pressure gradient of water vapor and plays a primary role as the driving force for the mass transport. Liquid-to-vapor and vapor-to-liquid phase transformations occur at the feed–membrane and membrane–permeate interfaces, respectively. Water molecules evaporate on the feed-side pore surface (inlet), migrate through hydrophobic membrane pores, and condense at the permeate-side membrane interface. The availability of low grade heat makes it possible, in combination with various heat sources, to extract high purity water from the feed solution. Comprehensive reviews for fundamental and practical aspects of membrane distillation processes can be found elsewhere [3–6].

Unlike pressure-driven membrane processes, DCMD is thermodynamically complex because mass, heat, and momentum transports are simultaneously involved to generate steady mass flux of water vapor. Vapor migration through membrane pores is governed by two major transport mechanisms, Brownian and Knudsen diffusion, as the viscous flow effects are often negligible in DCMD processes [7]. The complexity of the transport is due to the temperature gradient across the membrane pore causing diffusion coefficients to vary with the axial profile of the membrane temperature. Along the membrane pore, the gas phase of the vapor–air mixture must be in local thermodynamic equilibrium with the membrane wall of an axially varying temperature. Using the specific geometry of the membrane module (either plate-and-frame or hollow fiber), the Navier–Stokes equation must be solved first with the continuity equation, and the obtained flow field is used in the heat and mass transfer equation in membrane modules or channels [8]. The computational fluid dynamics is a generally sophisticated task so that it is often partially replaced using empirical correlations of heat/mass transfer. Fick's law governs the water vapor flux through the membrane pores, as water vapor and air molecules undergo interdiffusion by exchanging their positions in opposite directions. Assuming the gaseous

* Corresponding author at: Department of Civil and Environmental Engineering, University of Hawaii at Manoa, 2540 Dole Street, Honolulu, HI 96822, USA. Tel.: +1 808 956 3718; fax: +1 808 956 5014.
E-mail address: AlbertSK@hawaii.edu

0376-7388/$ - see front matter © 2012 Elsevier B.V. All rights reserved.
http://dx.doi.org/10.1016/j.memsci.2012.10.054

water vapors in the pore spaces are not transiently compressed, the water vapor flux is equal to the vapor condensation rate, which can be interpreted as measurable mass flux from the hot feed to the cold permeate streams.

Theoretical research for DCMD in the literature typically uses the mean temperature to estimate the effective diffusion coefficient, incorporates boundary layer correlations for heat and mass transfer, and inversely calculates heat flux across the membrane. To the best of our knowledge, accurate mass and heat balances through a membrane pore has not been rigorously investigated, especially by analytically solving axial temperature, diffusivity and concentration profiles. In the present work, we therefore scrutinized the microscopic transport phenomena using phase equilibrium theory, i.e., Clausius–Clapeyron equation and effective diffusion theory [9] to determine pressure and concentration of profiles in the membrane pore as a function of the axial distance from the pore inlet. Permeate flux is predicted using input temperatures of the feed and permeate streams and thermodynamic properties of liquid water, water vapor, and membrane.

2. Background study

To understand the current state-of-the-art of the DCMD process, this section briefly reviews theoretical and modeling status of the DCMD in terms of heat and mass balances. Fig. 1 shows a schematic of a straight pore structure of a porous membrane. Usually, a counter-current flow is maintained across the membrane to minimize heat loss: hot water of temperature T_1 is introduced in the (left) feed side and cold water of temperature T_4 flows in the permeate side in the opposite direction. The primary advantage of this counter-current flow setup is that the temperature gradient is almost constant over the membrane length between the two flows. After liquid water evaporates at the feed–membrane interface of temperature T_2, water vapor migrates through the membrane pore due to the partial pressure gradient (equivalent to vapor concentration), and finally condenses at the membrane–permeate interface of temperature T_3. Hydrophobicity of membrane materials effectively prevents viscous flow of liquid water through membrane pores unless the hydraulic pressure is high enough to cause the membrane wetting phenomena.

2.1. Heat transfer

From the hot feed to cold permeate, thermal zones can be classified in to three regions as shown in Fig. 1: (1) from the bulk feed of temperature T_1 to the feed–membrane interface of T_2, (2) from the feed–membrane interface (i.e., the pore inlet) to the membrane–permeate interface (i.e., pore outlet) of T_3, and (3) from the membrane–permeate interface to the bulk permeate of T_4 [6]. In these three regions, heat fluxes may be

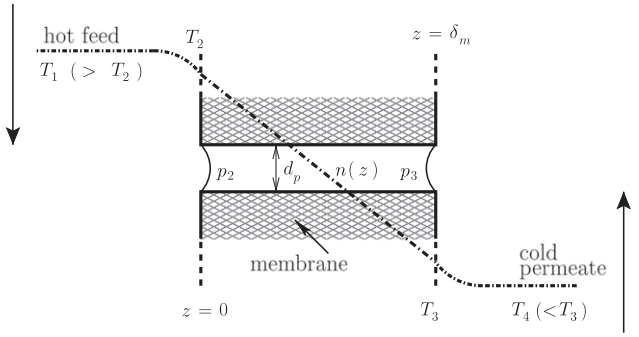

Fig. 1. Schematic diagram of counter-current direct contact membrane distillation system. The membrane pore has diameter d_p and length δ_m. T_1 and T_2 are temperatures of the bulk feed and on the feed–membrane interface at $z=0$, respectively; and T_3 and T_4 are temperatures on the membrane–permeate interface and of the bulk permeate, respectively. p_2 and p_3 are water–vapor pressures of the feed and permeate interfaces of the membrane pore, respectively, and $n(z)$ is the concentration of the gaseous water vapor.

$$Q_f = h_f(T_1 - T_2) \tag{1}$$

$$Q_m = h_m(T_2 - T_3) + J_w H_w = h'_m(T_2 - T_3) \tag{2}$$

$$Q_p = h_p(T_3 - T_4) \tag{3}$$

where h_f and h_p are the boundary layer heat transfer coefficients of the feed and permeate streams, respectively, h_m is the heat transfer coefficient of the porous membrane, H_w is the molar heat of water vaporization (also called evaporation enthalpy), and J_w is the molar flux of water vapor through the membrane pore.

In a steady state, the heat transfer in each region must be equal to each other: $Q_f = Q_m = Q_p = Q = \text{constant}$, and therefore Eqs. (1)–(3) can be re-organized to represent the heat flux in terms of the temperature difference between the feed and permeate

$$Q = \frac{T_1 - T_4}{\left(\frac{1}{h_f} + \frac{1}{h'_m} + \frac{1}{h_p}\right)} \tag{4}$$

where $h'_m = h_m + J_w H_w/(T_2 - T_3)$. Knowing that J_w is also a constant in a steady state, H_w can be estimated using the mean temperature of T_2 and T_3, or approximately T_1 and T_4. Eq. (4) is quantitatively valid if h_f, h_m, h_p, and H_w are not sensitively changing with temperature variation in each thermal region.

Owing to the boundary layer heat transport at both interfaces (at $x=0$ and $x=\delta_m$), the temperature inequality holds in general for $T_1 > T_2$ and $T_3 > T_4$, which indicates that the transmembrane temperature gradient, $T_2 - T_3$, contributing to the net transport of water vapor in the membrane pore, is less than the overall temperature difference between feed and permeate. Relationships between T_1 and T_2 and T_3 and T_4 can be obtained using empirical correlations of heat transfer across the membrane of length L in a general form of

$$\text{Nu} = \frac{h d_h}{k} = f\left(\text{Re}, \text{Pr}, \text{Gr}, \frac{d_p}{L}\right) \tag{5}$$

where Re, Pr, and Gr are Reynolds, Prandtl, and Grashof numbers. Details of this correlation can be found elsewhere [5], and [10] suggested a correlation $\text{Nu} = 0.74\,\text{Re}^{0.2}\,\text{Gr}^{0.1}\,\text{Pr}^{0.3}$ that provides the best fit of DCMD experimental data using a plate-and-frame module in laminar flow. In this study, we used the Dittus–Boelter type correlation suggested by [7].

An exact temperature profile can be obtained by solving a governing heat transfer equation of a differential form. Temperature decreases exponentially from T_2 at $z=0$ to T_3 at $z=\delta_m$. Diffusive heat flux due to vapor transport is much smaller than the conductive heat transfer through the solid part of the membrane. In this case, one can make an approximate linear temperature profile as

$$T(z) \backsimeq T_2 - \left[\frac{Q - (\overline{H_0} - \overline{c}_p T_2) J_w}{\overline{k}}\right] z \tag{6}$$

and the total heat flux across the porous membrane as

$$Q = h_m \times (T_2 - T_3) + (\overline{H_0} - \overline{c}_p T_2) J_w \tag{7}$$

where $h_m = \overline{k}/\delta_m$ is the effective heat transfer coefficient across the membrane. (See Appendix A.2 for details.) Note that the axial temperature profile $T(z)$ and the heat flux Q monotonously increase with respect to the molar flux J_w. The linear temperature profile of Eq. (6) is primarily due to the thin membrane thickness,

which is well-known in DCMD research. A thick DCMD membrane may cause exponentially decreasing temperature with respect to the axial coordinate z. Although the conventional linear temperature approximation is quantitatively valid as proven above, prediction of Q (from the bulk feed of T_1 to the bulk permeate of T_4) requires accurate prediction of J_w as a function of interface temperatures, T_2 and T_3: $J_w = J_w(T_2, T_3)$.

2.2. Mass transfer

In steady state, the permeate flux is equivalent to the condensation rate, i.e., the mass of vapor condensed per unit time and unit cross sectional area of the membrane pore. This permeate flux must be equal to the water vapor flux (J_w) from the feed–membrane to membrane–permeate interfaces of the membrane pore. It is often assumed that J_w is proportional to the partial pressure difference of water vapor. At thermodynamic equilibrium, vapor pressure (denoted in this study as p) replaces the partial pressure [11]:

$$J_w = C_m[p_2 - p_3] \tag{8}$$

where C_m is the membrane mass transfer coefficient, and p_2 and p_3 are vapor pressures of water proportional to concentrations, $n_2 = n(z=0)$ and $n_3 = n(z=\delta_m)$, respectively. The total pressure in the membrane pore must be the sum of partial pressures of water vapor and air, which is at least $P_{\text{atm}} = 1.0$ atm. Because temperatures at the feed and permeate sides are easier to measure instead of the partial pressure, the flux Eq. (8) can be transformed using temperature differences [12]

$$J_w = C_m \frac{dp}{dT}[T_2 - T_3] \tag{9}$$

In Eq. (9), dp/dT represents the variation of vapor pressure at a liquid–gas (i.e., water–vapor) equilibrium interface of a constant temperature T, which is called the Clausius–Clapeyron equation. In addition, C_m depends on temperature along the membrane pore. Using Eqs. (7) or (8) implicitly compels a representative temperature, at which C_m and $C_m(dp/dT)$ are calculated. Eq. (9) requires determining a representative temperature to evaluate $C_m(dp/dT)$ (or C_m in Eq. (8)). Without questioning, a good choice must be the average temperature $\overline{T}$ as discussed above. This approximation gives a simple equation to globally estimate the molar flux of water vapor through a membrane pore; however, the fundamental flaw implicitly included in Eq. (9) is from the fact that the Clausius–Clapeyron equation holds its validity only for a liquid–gas equilibrium at a specific temperature. This clarifies that dp/dT should be evaluated individually at the membrane interfaces at temperatures T_2 and T_3. Eqs. (8) and (9) imply that the membrane is thin enough to replace gradients of pressure and temperature by their differences divided by the membrane thickness. In this case, use of $C_m(dp/dT)|_{T=\overline{T}}$ forcefully assumes that the molar flux of water vapor is linearly proportional to the temperature or partial pressure gradient. However, to investigate local microscopic transport phenomena along the membrane pore these restrictive assumptions must be relaxed and/or verified. In our opinion, differential forms of mass and heat transfer equations should be used as governing equations to study the local transport phenomena.

3. Theory

3.1. Mass transport through membrane pores

In theoretical research on DCMD processes, heat and mass transport phenomena were researched using overall balances assuming steady state and/or equilibrium in three regions: feed, membrane, and permeate. Variations of thermodynamic quantities along the membrane pore must provide fundamental aspects of DCMD transport phenomena as well as accurate predictions of the performance, which have yet to be thoroughly studied to the best of our knowledge. Important physical quantities include latent heat of water, described by Clausius–Clapeyron equation, and mean free path of water vapor. (See Appendix A.1 for details.)

3.1.1. Generalized Fick's law with effective diffusion coefficient

Bosanquet proposed an expression to describe the effective diffusivity as a combination of Brownian and Knudsen diffusion coefficients

$$\frac{1}{D_e} = \frac{1}{D_B} + \frac{1}{D_K} \tag{10}$$

This relationship is analogous to two resistances connected in series in an electric circuit if the diffusivity inversed is interpreted as resistance [13,14]. Engineers have used a convenient empirical formula for water vapor diffusivity in air

$$D_B\ (\text{m}^2\ \text{s}^{-1}) = BT^{1+\alpha} \tag{11}$$

where $\alpha = 1.072$, $B = 1.895 \times 10^{-5}/P_T$ (Pa), and P_T is the total pressure of the gas phase in which water vapor is diffusing. The Knudsen diffusion coefficient is represented as [15]: $D_K = K\sqrt{T}$ where $K = \frac{1}{3} d_p \sqrt{8R/\pi m_w}$. Because membranes used for the DCMD process have sub-micron pore sizes, it is generally hard to determine the relative dominance between Brownian and Knudsen diffusion. We specify the effective diffusivity using Eq. (10) as

$$\frac{1}{D_e} = \frac{1}{BT^{1+\alpha}} + \frac{1}{K\sqrt{T}} \tag{12}$$

The overall effective diffusivity can be calculated as the inverse of integration of $1/D_e$ over the membrane length δ_m using the axial temperature profile. (See next section for details.)

The equilibrium states must be maintained separately at the inlet and outlet of the membrane pore with different temperatures. The use of the mean temperature between feed and permeate to evaluate the proportionality in Eqs. (8) and (9) can be improved by adopting a more rigorous governing equation. We propose using the molar flux equation in the original differential form of Fick's law

$$J_w = -D(T)\frac{dn}{dz} \tag{13}$$

and representing the linear temperature profile along the membrane pore of length δ_m as

$$T(z) = T_2 - \frac{\Delta T_m}{\delta_m} z \tag{14}$$

where $\Delta T_m = T_2 - T_3 > 0$ is the temperature difference between membrane interfaces, from which Q can be accurately calculated. The effective diffusivity is an implicit function of the axial coordinate because the temperature decreases with z. Integration of Eq. (13) from $z=0$ to $z=\delta_m$ and applying boundary conditions of $n(z=0)=n_2$ and $n(z=\delta_m)=n_3$ leads to

$$-\int_{z=0}^{z=\delta_m} \frac{1}{D(T)}\, dz = \frac{n_3 - n_2}{J_w} \tag{15}$$

because J_w is a constant in the steady state and therefore represented as

$$J_w = \frac{n_2 - n_3}{\delta_m} \frac{1}{\langle D^{-1} \rangle} \tag{16}$$

where $\langle D^{-1} \rangle$ is the mean of the inverse diffusivity over the membrane pore length calculated as

$$\langle D^{-1} \rangle = \frac{1}{\delta_m} \int_{z=0}^{z=\delta_m} \frac{1}{D}\, dz \tag{17}$$

The overall effective diffusivity can be approximated as $D_e = 1/\langle D^{-1}\rangle$ as a function of the interface temperatures, T_2 and T_3, which are between T_1 and T_4 due to the temperature polarization.

We substituted the linear temperature profile of Eq. (14) into Eq. (17) and used the chain rule to give

$$\langle D^{-1}\rangle = \frac{1}{\delta_m}\int_{z=0}^{z=\delta_m}\frac{1}{D(T)}\frac{dz}{dT}\,dT = \frac{-1}{\Delta T_m}\int_{T_2}^{T_3}\frac{1}{D(T)}\,dT \tag{18}$$

which requires an explicit representation of the diffusivity D as a function of temperature T. Substitution of Eq. (12) into (18) derives the length-averaged effective diffusivity as

$$D_e = \frac{1}{\langle D^{-1}\rangle} = \frac{T_2-T_3}{\frac{1}{\alpha B T_2^{\alpha}}\left(\left(\frac{T_2}{T_3}\right)^{\alpha}-1\right)+\frac{2\sqrt{T_3}}{K}\left(\sqrt{\frac{T_2}{T_3}}-1\right)} \tag{19}$$

whose validity can be checked by taking the mathematical limit of $T_2-T_3=\Delta T_m\to 0$:

$$\frac{1}{D_e} = \frac{1}{BT_2^{1+\alpha}}+\frac{1}{K\sqrt{T_2}} \tag{20}$$

which is identical to Eq. (12) at $T=T_2=T_3$.

The final analytic expression of the vapor flux through the membrane pore is calculated by substituting Eq. (19) into (16)

$$J_w = \frac{T_2-T_3}{\left[\frac{1}{\alpha B}(T_3^{-\alpha}-T_2^{-\alpha})+\frac{2}{K}(\sqrt{T_2}-\sqrt{T_3})\right]}\frac{n_2-n_3}{\delta_m} \tag{21}$$

Functional dependence of $n(T)$ on temperature T can be found in Appendix A.1. Note that the molar flux J_w is proportional to not only the concentration gradient $(n_2-n_3)/\delta_m$ but also to the feed and permeate temperatures, T_2 and T_3, independently. D_e cannot be represented as a sole function of ΔT_m. If one assumes that the water vapor follows the ideal gas law, $p=n_w k_B T$, and expresses the vapor pressure p using the Clausius–Clapeyron equation, then the gaseous concentration of water vapor can be easily calculated. (See Appendix A.1 for details.) Along the membrane pore the temperature is approximately linear, but the vapor pressure and concentration increases non-linearly. This implies that using the mean temperature across the membrane pore provides erroneous estimation of p and dp/dT. The number concentration gradient is then

$$\frac{n_2-n_3}{\delta_m} = \frac{1}{\delta_m k_B}\left(\frac{p_2}{T_2}-\frac{p_3}{T_3}\right) = \frac{p_0}{\delta_m k_B}\left(\frac{e^{-L(T_2)/RT_2}}{T_2}-\frac{e^{-L(T_3)/RT_3}}{T_3}\right) \tag{22}$$

A full mathematical representation of the mass flux J_w can be obtained by substituting Eq. (22) into (21), which is omitted due to mathematical complexity. The newly developed molar flux Eq. (21) indicates that the vapor flux in turn has a complex functional form of (individual) T_2 and T_3, which independently controls the vapor pressures and concentrations at the pore inlet and outlet interfaces, respectively. The water latent heat and vapor pressure must be paid equal attention to because the latent heat controls the partial pressure of water vapor as well as heat conduction through membrane pores. The dominance of a diffusion mechanism, Knudsen over Brownian or vice versa, can be alternatively investigated using B and K instead of the Knudsen number Kn with a representative temperature.

3.1.2. Molar flux across the membrane

Note that J_w expresses the mole number of water vapor passing through the cross sectional area of the membrane pore, πd_p^2, per unit time. Within the porous membrane, water vapor can migrate through the detoured void spaces and therefore the net permeate flux to be compared with experimental data is

$$J_p = \frac{\epsilon}{t_m}J_w \tag{23}$$

where t_m is the diffusive tortuosity indicating the reduced diffusion due to the non-straight pore paths of the membrane. Using Maxwell's equation [16], we estimate the diffusive tortuosity as

$$t_m = 1+\tfrac{1}{2}(1-\epsilon) \tag{24}$$

of which values are 1.2 and 1.1 for $\epsilon=0.6$ and 0.8, respectively. Fundamental discussion of the diffusive tortuosity and effects of pore structure on the Knudsen diffusion can be found elsewhere [17,18]. Because T_2 and T_3 are not directly measurable, they must be theoretically determined using the heat transfer coefficients $h_f(T_1)$ and $h_p(T_4)$, respectively. In addition, the membrane heat transfer coefficient h_m should be measurable or be available from vendors.

The iterative procedure to calculate J_p is as follows:

1. Assume $T_2(<T_1)$.
2. Calculate $T_3 = T_4+\frac{h_f}{h_p}\times(T_1-T_2)$.
3. Calculate J_w of Eq. (21) using T_2 and T_3 obtained above.
4. Calculate the overall heat flux using Eq. (7).
5. Update $T_2 = T_1-Q/h_f$.
6. Go to step 2 unless T_2 converges in this iteration.
7. Calculate J_p using converged J_w.

3.2. Required power per flux

Consistent availability of a heat source to maintain feed temperature T_1 is the primary requirement to be met for steady-state operation of DCMD. The constant vapor flux J_w implies heat energy is consumed as much as to transform the liquid water to water vapor. Eq. (4) indicates that as the mass flux J_w increases, $1/h'_m$ decreases so that the heat flux increases. As the transformation of water from liquid to gas phases is the primary physical phenomena during MD processes, it is important to estimate how the vapor flux does influence the heat lost per time. When performance of two membranes is compared, one providing a higher vapor flux will consume more heat energy from the feed stream of T_1. Therefore, it is worth calculating variation of heat flux with respect to vapor flux to analyze thermal performance of DCMD. We differentiate both sides of Eq. (7) (instead of Eq. (2)) with respect to J_w for the heat transfer rate through the membrane pore to calculate

$$\frac{\partial Q}{\partial J_w} = \overline{H}_0-\overline{c}_p T_2-J_w\overline{c}_p\frac{\partial T_2}{\partial J_w}+\overline{h}_m\frac{\partial(T_2-T_3)}{\partial J_w} \tag{25}$$

Because T_1 and T_4 are constant, Eqs. (1) and (3) suggest

$$\frac{\partial Q}{\partial J_w} = -h_f\frac{\partial T_2}{\partial J_w} = +h_p\frac{\partial T_3}{\partial J_w} \tag{26}$$

Substitution of Eq. (26) into (25) gives

$$\frac{\partial Q}{\partial J_w} = \frac{\overline{H}_0-\overline{c}_p T_2}{h_m(h_f^{-1}+h_m^{-1}+h_p^{-1})-J_w\overline{c}_p h_f^{-1}} \tag{27}$$

which implies that, per mass flux, more heat is consumed if vapor flux J_w increases and/or temperature at the feed membrane interface, T_2, decreases. Since T_2 is proportional to T_1, Eq. (27) indicates that less heat is required as the feed temperature increases.

3.3. Pore size distribution

Pore sizes of membranes usually follow log-normal distribution, expressed as

$$\mathcal{L}(d_p) = \frac{1}{sd_p\sqrt{2\pi}}e^{-(\ln d_p-m)^2/2s^2} \tag{28}$$

and its cumulative function is

$$\mathcal{F}(d_p) = \frac{1}{2}\left[1+\mathrm{erf}\left(\frac{\ln d_p - m}{s\sqrt{2}}\right)\right] \tag{29}$$

where m and s are parameters of the log-normal distribution, and erf is the error function: $\mathrm{erf}(x) = 2\pi^{-1/2}\int_0^x e^{-t^2}\,dt$. The dominance of diffusion mechanisms varies with pore sizes, and therefore the average vapor flux can be estimated as

$$\langle J_w \rangle = \int_0^\infty J_w \mathcal{L}(d_p) d_p \tag{30}$$

Vapor flux Eq. (21) includes only K proportional to d_p (i.e., $K = d_p\eta$ where $\eta = \frac{1}{3}\sqrt{8R/\pi m_w}$), which can be represented as a power series of K/B, if Brownian diffusion suppresses Knudsen diffusion, as

$$J_w^B \backsimeq \frac{B(T_2-T_3)}{2(\sqrt{T_2}-\sqrt{T_3})}\left[\left(\frac{K}{B}\right)-\left(\frac{K}{B}\right)^2\frac{(T_3^{-\alpha}-T_2^{-\alpha})}{2\alpha(\sqrt{T_2}-\sqrt{T_3})}\right]\frac{n_2-n_3}{\delta_m} \tag{31}$$

On the other hand, Eq. (31) is expanded as a series of K/B. If the Knudsen diffusion is dominant, the vapor flux is limited by Brownian diffusion so that

$$J_w^K \backsimeq \frac{\alpha B(T_2-T_3)}{(T_3^{-\alpha}-T_2^{-\alpha})}\left[1-2\alpha\left(\frac{B}{K}\right)\frac{(\sqrt{T_2}-\sqrt{T_3})}{(T_3^{-\alpha}-T_2^{-\alpha})}\right]\frac{n_2-n_3}{\delta_m} \tag{32}$$

For Eqs. (31) and (32), calculation of pore-size-averaged fluxes requires calculating

$$\langle d_p^{-1}\rangle = e^{-m+(1/2)s^2} = \langle d_p\rangle e^{-2m} = e^{s^2}/\langle d_p\rangle \tag{33}$$

$$\langle d_p\rangle = e^{m+(1/2)s^2} \tag{34}$$

$$\langle d_p^2\rangle = e^{+2m+2s^2} = e^{s^2}\langle d_p\rangle^2 \tag{35}$$

The standard deviation of pore sizes is then

$$\sigma_p = \sqrt{\langle d_p^2\rangle - \langle d_p\rangle^2} = \sqrt{e^{s^2}-1} \tag{36}$$

so that, if $s=0$, pores are completely mono-dispersed, i.e., $\langle d_p\rangle = d_p$. Substitution of Eqs. (31) and (32) into Eq. (30) further provides

$$\langle J_w^B\rangle \backsimeq \frac{\langle K\rangle^2(T_2-T_3)}{2(D_{K,2}-D_{K,3})}\left[1-\frac{\langle K\rangle^2}{2\alpha}\frac{(T_3D_{B,3}^{-1}-T_2D_{B,2}^{-1})}{(D_{K,2}-D_{K,3})}e^{s^2}\right]\frac{n_2-n_3}{\delta_m} \tag{37}$$

and

$$\langle J_w^K\rangle \backsimeq \frac{\alpha(T_2-T_3)}{(T_3D_{B,3}^{-1}-T_2D_{B,2}^{-1})}\left[1-\frac{2\alpha}{\langle K\rangle^2}\frac{D_{K,2}-D_{K,3}}{(T_3D_{B,3}^{-1}-T_2D_{B,2}^{-1})}e^{s^2}\right]\frac{n_2-n_3}{\delta_m} \tag{38}$$

respectively, where $D_{B,i} = D_B(T=T_i)$ and $D_{K,i} = D_K(T=T_i, d_p = \langle d_p\rangle)$ for $i=2$ and 3, and $\langle K\rangle = \langle d_p\rangle\eta$. In Eqs. (37) and (38), the second terms with s are smaller than one due to the dominance of diffusion mechanisms, which suggests that polydispersity of pore sizes always provides a smaller vapor flux than that of monodispersed pore size of $d_p = \langle d_p\rangle$.

4. Results and discussion

4.1. Diffusivity of water vapor

An empirical correlation of Eq. (11) for the Brownian diffusivity of water vapor has been reported by [19] and discussed in Ref. [20]. Phattaranawik et al. [21] used this relationship to predict the molar flux of water vapor through membrane pores. Eq. (11) requires information of the total pressure. Two estimates are reasonable for the total pressure in the membrane pore: (i) $P_T = P_{\mathrm{atm}} = 1.0$ atm and (ii) $P_T = P_{\mathrm{atm}} + \frac{1}{2}p_2$ where $p_2 = p(T_2)$. The first assumption of $P_T = 1$ atm is equivalent to set (mathematically) $T_2 = 0$ °C for the vapor pressure calculation. As the pore is initially in 1 atm before any evaporation on condensation, the total pressure in the DCMD state can be (in principle) higher than 1 atm. This should be considered carefully. The assumption of constant J_w indicates continuous evaporation at the pore inlet, of which rate is driven by the difference between actual pressure of the gas phase at $z = 0^+$ (inside the pore inlet) and the vapor pressure of water at $T = T_2$. If a thermodynamic equilibrium is kept at the pore inlet, then no evaporation occurs. Vapor pressure was used to estimate the vapor concentration using the ideal gas law. Although J_w is phenomenologically constant, DCMD processes are, rigorously saying, in non-equilibrium states. The compensation is the total pressure inside the membrane pore higher than 1.0 atm, however the quantification below indicates the difference is small and so does not affect the vapor diffusion too much. The above assumption may provide a higher upper limit of P_T because $P(T)$ increases with respect to temperature in a non-linear fashion. Fig. 2 shows effects of temperature on Brownian, Knudsen, and effective diffusion coefficients.

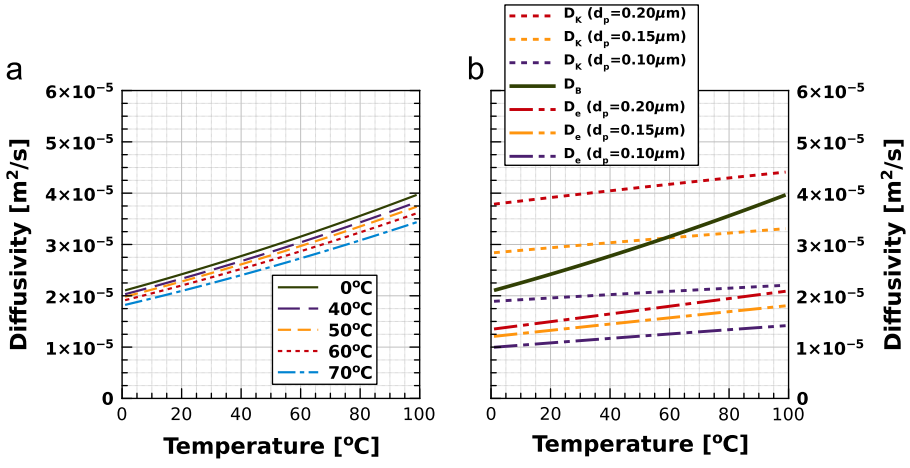

Fig. 2. Diffusion coefficients versus temperature: (a) Brownian diffusion coefficient of Eq. (11) with the total pore pressure assumed $P_T = p_a + \frac{1}{2}p_w(T_2)$ using T_2 values of 0, 40, 50, 60, and 70 °C, where $T_2 = 0$ °C indicates the pore pressure is 1.0 atm and (b) effective diffusion coefficient calculated using Eq. (10) with pore diameters of 0.10, 0.15, and 0.2 μm. In figure (b), the dotted lines indicate the Knudsen diffusion coefficients with the three pore diameters; the solid line is the Brownian diffusivity at 1.0 atm; and the dash-dot lines correspond to effective diffusion coefficients calculated using Eq. (10). Decreasing temperature from feed to permeate interfaces is equivalent to increasing axial distance z from 0 to δ_m as indicated in Eq. (6).

We take the second (flexible and general) assumption, estimate the total pressure at temperature 0, 40, 50, 60, and 70 °C, and calculate the Brownian diffusivity as shown in Fig. 2(a). These inlet temperature values are only to estimate the total pressure that is not accurately known in the membrane pore. The Brownian diffusivity does not significantly change with the inlet temperature, because the total pressure variation, $\frac{1}{2}p_2$, is very slow. If the feed temperature is 70 °C, the water vapor pressure on the feed side of the membrane is as much as 234 mmHg, making the total pressure approximately $760+0.5\times234=877$ mmHg. This increase is only about 15% from the initial atmospheric pressure. Therefore, the water vapor pressure does not significantly increase the total pressure in the membrane pore during non-equilibrium DCMD processes. The feed temperature below 40 °C requires additional cooling of the permeate stream and heating of the feed stream to higher than 80 °C. Inclusion of $\frac{1}{2}p_2$ in the total pressure decreases the Brownian diffusivity only about 10% from that of $P_T=1.0$ atm as shown in Fig. 2(b). Therefore, for the rest of calculation, we used $P_T=1$ atm for simplicity. The Knudsen diffusivity is less sensitively increasing with respect to the temperature as compared to the Brownian diffusivity of Eq. (11). Note that $D_B\propto T^{2.072}$ and $D_K\propto T^{0.5}$. The dominance of D_K over D_B is truly dependent on the membrane pore sizes. In the entire temperature range from 0 to 100 °C, D_B is fully bounded between $D_K(d_p=0.1\ \mu m)$ and $D_K(d_p=0.2\ \mu m)$, which implies that a small changes in membrane pore sizes can easily switch the primary diffusion mechanism between Brownian and Knudsen. For $\lambda\simeq0.1\ \mu m$, $K_n=0.1$ and 10 indicate $d_p=1\ \mu m$ and 0.01 μm, respectively, which can fully cover the pore size distribution of DCMD membranes. When the membrane surface has a pore size distribution, the dominant mechanism of the diffusive transport must be topologically localized. Use of mean pore size can be a good approach to predict the mean molar flux along a pore using the representative diameter, but estimation of the total molar flux as the sum of Knudsen-dominant and Brownian-dominant fluxes with assigned fractions (based on the Knudsen number or equivalent) is perhaps a better approximation [22].

The Bosanquet approximation of Eq. (10) is equivalent to resistances in series because the inverse of each diffusion coefficient is added. Often researchers considered fraction on each diffusivity coefficient, which may increase better prediction. The effective diffusion coefficient is, therefore, always smaller than any other and closer to the smaller of Brownian or Knudsen diffusion coefficients. Given a pore size, the effective diffusivity shown as dash-dot lines in Fig. 2(b) are always below both Brownian diffusivity and Knudsen diffusivity. The qualitative assumption of the constant total pore pressure plays a very important role, which significantly simplifies theoretical development by eliminating viscous flow effects. The experimental verification of the negligible viscous flow reported by [7] emphasizes that, from the ideal gas law, the total gas concentration n_T increases along the membrane pore as the temperature decreases from the feed to permeate streams: $P_T=\text{constant}=n_Tk_BT=C_TRT$, where C_T is the total molar concentration. The total concentration increases as the temperature decreases along the pore: $n_T\propto1/T(z)$. A higher molecular concentration near the pore outlet at T_3 provides more frequent collision opportunities to traveling water vapor molecules because the mean free path is inversely proportional to the concentrations. As a consequence, the effective diffusivity must decrease along the membrane pore. The transport phenomena can be described as follows in terms of the linear temperature decrease from the pore inlet to the outlet. First, on the feed–membrane of T_2 (which is higher than T_3), water vapor molecules are produced at the non-equilibrium interface between liquid and gas; and the molecular kinetic energy proportional to k_BT_2 contributes to faster molecular speed and higher diffusion coefficients. Second, with negligible viscous flow implying the pseudo-constant total pressure, the total concentration increases as the temperature decreases from the pore inlet to the outlet; and therefore at the membrane–permeate interface of T_3, molecules have less kinetic energy and more opportunities to collide with other molecules. Third, the mean free path decreases along the membrane pore and must reach a minimum at the membrane–permeate interface. (Refer to Fig. A3 in Appendix.)

4.2. Membrane vapor flux

Molar flux of water vapor through a membrane pore is calculated using Eq. (16) with Eqs. (19) and (22). The permeate flux of Eq. (23) is the final theoretical representation of the molar flux to be compared with experimental observation, which has a qualitative form:

$$J_p=Sj_w(T_1,T_4|h_f,h_p,\text{Kn}) \tag{39}$$

where, in this study, S is defined as a structural number of membrane distillation

$$S=\frac{\epsilon}{t_m}\cdot\frac{d_p}{\delta_m} \tag{40}$$

and j_w is defined as a specific molar flux

$$j_w=\frac{\delta_mJ_w}{d_p} \tag{41}$$

Note that the proportionality S is a single dimensionless number that includes the geometrical and structural information of membrane materials; and j_w is a function of d_p, T_1 and T_4 only. Note that h_f and h_p are functions of T_1 and T_4 and used to calculate the interface temperatures of T_2 and T_3, respectively. The Knudsen number Kn links the microscopic pore structure to molecular diffusion with axially decreasing membrane temperature. We compare our theoretical development with Lawson and Lloyd's [7] experimental observation using 3M membranes. Dittus–Boelter type correlation [7] was used to calculate heat transfer coefficients, $h_f(T_1)$ and $h_p(T_4)$

$$h[\text{W/m}^2\text{K}]=5122+76.63\times(T-T_0) \tag{42}$$

where T is the absolute temperature and $T_0=273.15$ K. Effects of salt concentration in the feed water (0.0, 0.6, and 1.3 mol%) were

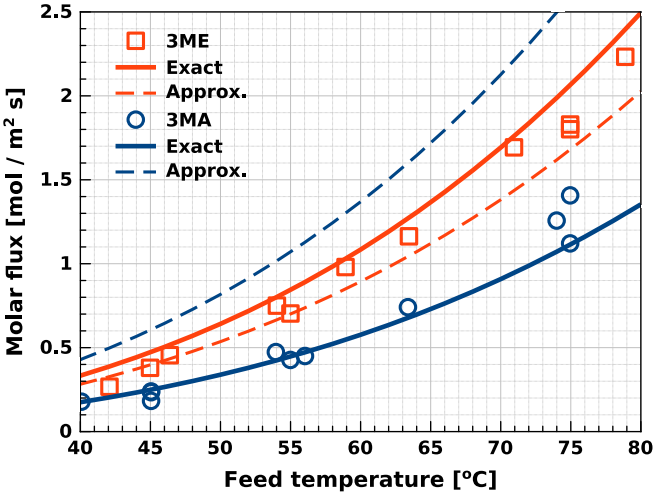

Fig. 3. Comparison of theoretical prediction of water vapor fluxes with experimental observation [7] with respect to the feed temperature at permeate temperature of 25 °C. Symbols and lines indicate experimental and theoretical results using 3MA ($\epsilon_{max}=0.66$, $d_p=0.29\ \mu m$ and $\delta_m=91\ \mu m$) and 3ME ($\epsilon_{max}=0.85$, $d_p=0.73\ \mu m$ and $\delta_m=79\ \mu m$) membranes.

investigated using 3MA and 3ME membranes; and the permeate flux was found to be insensitive to the feed salinity.

Fig. 3 compares molar fluxes predicted by our theory, the mean-temperature approximation, and measured by Lawson and Lloyd [7] regardless of salt concentrations of the feed stream. The permeate temperature was set for $T_4 = 25\ ^\circ C$. Our theoretical results well capture the trend of the vapor flux change with respect to the feed temperature. The current theory slightly underestimates (and overestimates) the vapor flux through 3MA (and 3ME) membranes. Because 3ME has thinner membrane dimension, larger porosity and bigger pore diameter than those of 3MA, its permeate flux is higher than that of 3MA. As the feed temperature varied from 40 to 80 °C, the overall temperature difference between the feed and permeate stream changed from 15 to 55 °C. Prediction accuracy of our theory is consistent over the entire temperature range. The molar flux of 3ME is about twice that of 3MA: $J_{p,3ME} \approx 2J_{p,3MA}$. Since the mean-temperature approximation does not include the axial variation of vapor pressure, concentration, and diffusive transport from the pore inlet to outlet, its prediction accuracy is not consistent as compared to results from the exact solution. For the 3ME membrane, the approximate approach underestimates the experimental observation of the vapor flux, which is between the exact and approximate predictions. For the 3MA membrane, the predicted flux by the approximate theory is twice as large as the experimental measurement and the exact theory. The primary reason of this inconsistent prediction trend is due to over-simplification of the two phase transformation at the pore inlet and outlet (for evaporation at T_2 and condensation at T_3, respectively) to a single representative transformation in the middle of the membrane channel at temperature $\overline{T} = \frac{1}{2}(T_2 + T_3)$. Because the temperature profile is monotonous along the membrane pore in most DCMD membranes (see Appendix A.2 for mathematical analysis), estimation of the mean temperature must be proper, but non-linearity of vapor pressure and concentration causes inaccurate estimation of proportional coefficients, C_m and $C_m(dP/dT)$, at the mean temperature $\overline{T}$, of Eqs. (8) and (9), respectively. (See Appendix A.1.5 for details about the flux calculation using the mean temperature.) The inaccuracy and inconsistency of the mean-temperature approximation is very noticeable for the 3MA membrane case, which has lower porosity, smaller pore size, and longer pore length. The length-to-diameter ratio of a membrane pore can be an important criteria that can determine the applicability of the mean-temperature approximation. 3MA and 3ME membranes have δ_m/d_p ratios of 314 and 108, respectively. This implies that, for two membranes of the same pore size and different lengths, the mean-temperature approximation will provide a better flux estimation for a thinner membrane that provides a stiffer temperature profile. The inconsistency of the approximation stems from the mandatory theoretical condition that the difference between T_1 and T_4 across a thin membrane should be small enough to linearize vapor pressure, which is not always satisfied in the experimental conditions. As Eqs. (39)–(41) indicate, effects of the structural number and interface temperatures are independent. Knudsen numbers of 3MA and 3ME membranes are approximately 0.345 and 0.137, respectively, which are in the transition region: $10^{-1} < \mathrm{Kn} < 10$. Fig. 2(b) implies that Knudsen transport dominates Brownian diffusion so that the limiting transport mechanism is due to random collisions between diffusing molecules. Influences of membrane porosity and pore size on the vapor flux are similar to each other in 3MA and 3ME membrane cases, which suggests that the inaccuracy of the mean-temperature approximation for the 3MA membrane originates primarily from the pore length, i.e., membrane thickness. As indicated above, the temperature profile is linear along the membrane pore, which is typically smaller than 100 μm in DCMD processes [2]. As the membrane thickness increases, non-linearity effects of vapor concentration and dominance of the transport mechanism in the axial direction becomes predominant. Taking a mean temperature to roughly estimate the transport coefficient C_m or the Clausius–Clapeyron term dP/dT does not always provide a good guess for quantitatively accurate prediction of the vapor flux. This analysis implies that the mean-temperature approximation can be used for thin membranes, which phenomenologically generate axially monotonous profiles of vapor pressure, concentration, and temperature.

The structural numbers of these membranes are $S_{3MA} = 1.798 \times 10^{-3}$ and $S_{3ME} = 7.306 \times 10^{-3}$, which gives $S_{3ME}/S_{3MA} = 4.064$. This concludes that the specific flux of 3ME is about a half of that of 3MA: $j_{3ME} \approx \frac{1}{2} j_{3MA}$, which is primarily influenced by the effect of relative pore sizes of 3MA and 3ME membranes when the feed and permeate temperatures are constant. Note that j_w is not dependent on δ_m but decreases with d_p. The inverse-diameter ratio of 3ME and 3MA is $d_{p,3MA}/d_{p,3ME} = 0.29/0.73 = 0.40$. Then, the product of ratios of structural number and inverse diameter is $4.064 \times 0.40 = 1.626$, which is close to an accurate molar flux ratio of 3ME and 3MA. This gives a practically important fact when comparing performance of two membranes. The porosity per membrane thickness, δ_m/ϵ, characterizes how much void spaces are available for vapor–air interdiffusion followed by heat conduction per membrane thickness while d_p controls the dominant diffusion mechanism.

Fig. 4 shows the permeate fluxes plotted with respect to the temperature difference between feed and permeate with given feed temperatures of 41, 59, and 79 °C. Increasing the temperature difference (specifically in this case) has roughly equivalent impact of decreasing the permeate temperature with a constant feed temperature. Given a temperature difference, a higher feed temperature provides a higher flux by producing more water vapor molecules of higher kinetic energy at the liquid water interface. *When two MD processes of different feed temperatures are set, one with a higher feed temperature requires less temperature gradient along the membrane pore of the same length; or if the same temperature gradient is maintained with different permeate temperatures, one with a higher permeate temperature provides a higher flux*. This clearly indicates that the vapor flux is not a function of the temperature difference only, but of feed and permeate temperature individually (or equivalently feed (or permeate) temperature and temperature difference). Similar to the trend in Fig. 3, the mean-temperature approximation of Fig. 4 consistently underestimates the experimental observation for the three

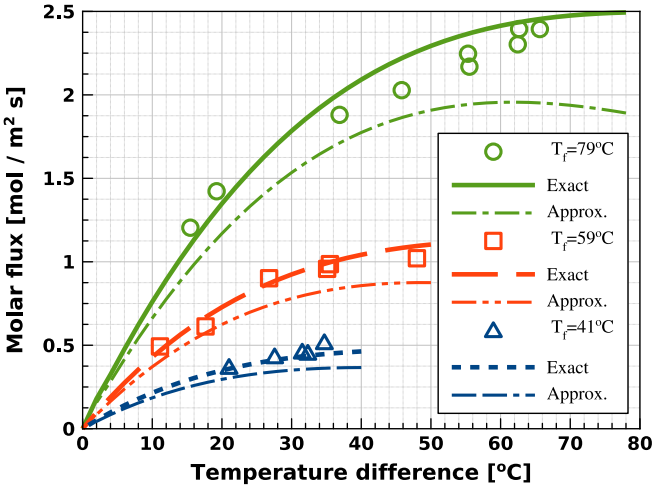

Fig. 4. Comparison of theoretical prediction of water vapor fluxes with experimental observation [7] with respect to the temperature difference at feed temperatures of $T_f = 79\ ^\circ C$, 59 °C, and 41 °C using 3ME membranes.

temperatures. More importantly, molar vapor fluxes in Fig. 4 seem to converge to a limiting value as the temperature difference increases, which is primarily due to the convective heat loss of Eq. (7), i.e., $(\overline{H}_0-\overline{c}_pT_2)J_w$. At permeate temperature T_4, as the feed temperature T_1 increases, total heat flux, T_2, T_3, and T_2-T_3 increase, generating higher vapor flux. At the same time, a part of total heat flux is taken through the solid part of the membrane, $h_m(T_2-T_3)$. Consequently, increasing T_1 contributes to conductive and the convective heat flux so that the vapor flux converges to a semi-plateau as the temperature difference approaches close to its theoretical maximum. Because the mean-temperature approximation uses only the temperature difference, Fig. 4 shows unphysical behavior of the vapor flux that reaches a maximum and decreases to the feed temperature. This quantitative inaccuracy must be more significant for thicker membranes. Figs. 3 and 4 change the feed and permeate temperatures with constant permeate and feed temperatures, respectively. In both cases the present theory agrees well with the experimental observations.

One should note that in the current theory the viscous flow is not included as a vapor transport mechanism. A quantitative analysis is as follows. For a laminar flow of a fluid of viscosity μ_f through a pore of diameter d_p and length δ_m, the average fluid velocity is

$$\langle v\rangle = -\frac{d_p^2}{32\mu_f}\frac{d\mathcal{P}}{dx} \approx \frac{d_p^2}{32\mu_f}\frac{|\Delta\mathcal{P}|}{\delta_m}$$

where $\mathcal{P}$ is hydrostatic pressure generating the average speed $\langle v\rangle$. We take sample parameters to estimate $\langle v\rangle$ from Fig. 3: 3MA membrane has $d_p = 0.73$ μm and $\delta_m = 79$ μm. If we estimate $|\Delta P|$ as the water vapor pressure at mean temperature 50 °C, i.e., 100 mmHg = 13,332 Pa s, and use an air viscosity of $\mu_f = 20$ μPa s s for T = 300–350 K, then the average Poiseuillie's velocity is approximately

$$\langle v\rangle \approx \frac{(0.73\times10^{-6}\ \text{m})^2}{(32)(2\times10^{-5}\ \text{Pa s s})}\frac{1.33\times10^{4}\ \text{Pa s}}{79\times10^{-6}\ \text{m}} = 0.137\ \text{m/s}$$

The molar concentration of water vapor at 50 °C is around 4 mol/m^3, which provides the viscous mass flux, 0.137 m/s × 4 mol/m^3 = 0.55 mol/m^2 s. This value estimates well the measured vapor flux at feed temperature 55 °C as shown in Fig. 3, and a half of that at 75 °C. The mean temperature used here, 50 °C, is an arithmetic average of feed temperature 75 °C and permeate temperature 25 °C. This estimation indicates that addition of the viscous flow to the diffusive mass transport significantly overestimates the experimental observation; or the diffusive transport can be mathematically mapped as the Hagen–Poiseuillie flow. Several researchers included the viscous flow in DCMD, which is, however, a double-counting of the transport mechanism for a single physical phenomena. At the feed–membrane and membrane–permeate interfaces, phase transformation between liquid and gas phases naturally occur basically due to the global temperature difference, T_1-T_4. In other words, creation of vapor molecules at the pore inlet and its annihilation at the pore outlet provide a vapor concentration gradient in the form of the partial pressure, approximated as the vapor pressure. At any location within the pore, $0 < z < \delta_m$, the total pressure, i.e., the sum of partial pressures of water vapor and air is (approximately) equal to 1 atm so that no net total pressure gradient exists. At the pore inlet, the air-vapor mixture is not pushed hydraulically, but the diffusive vapor flux to the pore exit is compensated by the air flux in the opposite direction. Since there is no forceful hydraulic pressure gradient, the mass transport in DCMD is purely diffusive.

4.3. Energy consumption

Fig. 5 shows profiles of temperature at the two interfaces, T_2 and T_3, bounded between T_1 and T_4. T_1 increases from the permeate temperature T_4(= 20 °C). Temperature T_2 monotonously increases with feed temperature T_1, due to the conductive heat transport being dominant at the feed–membrane interface. As T_1 increases, the higher temperature difference (between feed and permeate) enhances the vapor flux carrying the evaporation heat of water so that the difference between T_1 and T_2 linearly increases with respect to T_1. On the other hand, convective heat transfer (with molar vapor flux J_w) in addition to conductive heat transfer contribute to enhance T_3 (at the membrane–permeate interface) when the vapor flux is very small. The enhanced temperature difference as a driving force enhances the vapor flux, which carries the evaporation heat from the feed to the permeate side (i.e., from pore inlet to outlet, respectively), and hence T_3. This increased T_3, i.e., temperature polarization, effectively reduces the overall temperature gradient and hence the net driving force to the vapor flux. Therefore, the vapor flux gradually increases with respect to the temperature difference as shown in Fig. 4. T_2 and T_3 under the conductive heat transfer only can be easily estimated using Eqs. (1)–(3) with $J_w \to 0$. This temperature polarization in MD plays a very similar role of concentration polarization in reverse osmosis and/or nanofiltration.

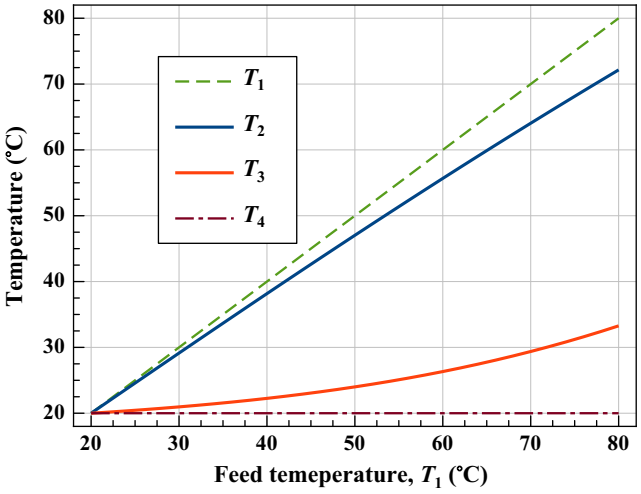

Fig. 5. Temperature profiles of 3ME membrane with respect to T_1.

Effect of feed temperature increase on the vapor flux is less sensitive for higher feed temperatures: the increment of flux per unit feed temperature is higher at low feed temperatures. Fig. 6 shows an almost linear dependence of total heat flux Q with respect to J_w. Although J_w varies with T_2 and T_3 in a non-linear manner, Eq. (7) implies that Q and J_w have a linear relationship, which is shown in Fig. 6(a). A derivative of Q with respect to J_w, meaning heat flux increase per unit vapor flux, shown in Fig. 6(b) expresses the rapid increase of Q at low vapor flux and gradual variation at high flux. This is because, at high feed temperature, the vapor flux carries more evaporation heat from the feed to the permeate side, and this carried heat increases T_3, reducing the increase rate of heat flux per vapor flux. Although this non-linear trend is obvious, variation of dQ/dJ_w over the range of J_w(0.0–2.5 mol/m^2 s) is very small, i.e., roughly 22.3–22.7 kJ/mol, which supports the monotonous variation of Q with respect to J_w as shown in Fig. 6(a).

4.4. Effects of pore size distribution on permeate flux

In this section, we qualitatively discuss effects of the pore size distribution on the vapor flux. Fig. 7 shows log-normal distributions of pore sizes with average diameters of 0.1 and 0.5 μm. Note that the vapor mean free path is about 0.1 μm. For the case of

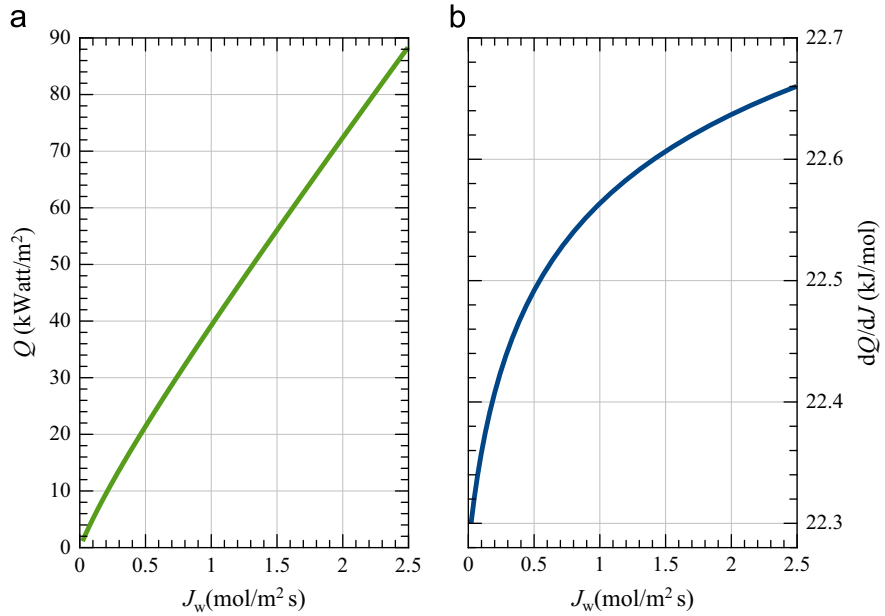

Fig. 6. (a) Heat flux Q and (b) its derivative with respect to vapor flux J_w.

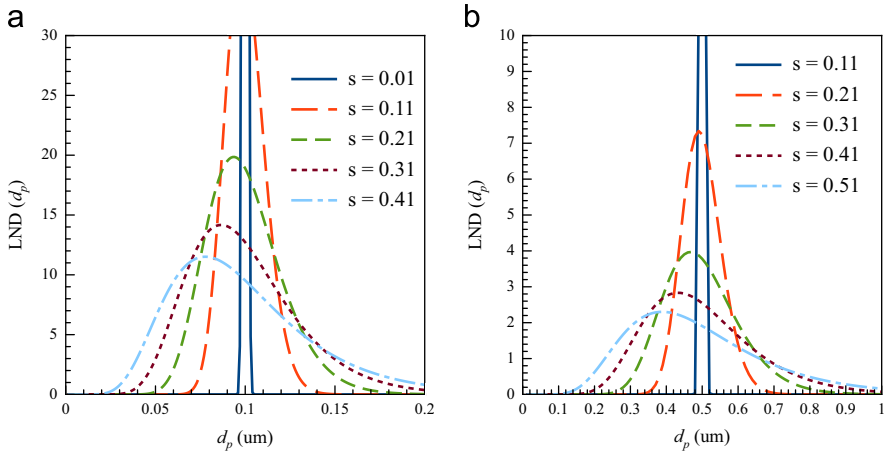

Fig. 7. Pore size distribution (a) $\langle d_p \rangle = 0.1$ μm and (b) $\langle d_p \rangle = 0.5$ μm with various s.

$\langle d_p \rangle = 0.1$ μm (Fig. 7(a)), the narrowest distribution of $s=0.01$ indicates that the Knudsen number is one, i.e., Kn=1. As s increases, the pore size distribution becomes broad and the peak moves left, which indicates the presence of more small pores. A broader distribution of pore sizes must generate less vapor flux than that of mono-dispersed distribution with the same mean pore size. As the pore size changes from 0.02 to 0.2 μm, the Knudsen number varies from 5 to 0.5 so that the dominant diffusion mechanism is not Brownian or Knudsen diffusion, but the diffusive transport mechanism is locally dominated along the membrane surface according to pore size distribution. Even if the mean pore size is much smaller than the vapor mean free path, i.e., $\langle d_p \rangle \ll \lambda (= 0.1\ \mu m)$. Eq. (37) indicates that a broad distribution ($s > 0$) provides smaller vapor flux than that of mono-dispersed pore sizes ($s = 0$). When the mean pore size is bigger than the mean free path (Fig. 7(b)), as the distribution becomes broader with increasing s, a larger number of small pores decreases the vapor flux (Eq. (38)). A very broad distribution (e.g., $s=0.51$) can have pore sizes close to the vapor mean free path (0.1 μm), at which the Knudsen number is on the order of $O(1)$. A small fraction of pore sizes of this distribution can have pore sizes close to or bigger than 1.0 μm, where the Brownian diffusion must be dominant. However, the presence of these few large pores may cause membrane wetting. In terms of the pore size distribution, a narrow distribution (i.e., $s \to 0^+$)with a specific mean pore size is a primary factor in minimizing the diffusive transport of water vapors through the membrane pore. To the best of our knowledge, the present work is the first to mathematically prove that the non-zero variance decreases the water vapor flux of DCMD processes.

Given physical properties of the porous membrane such as porosity ϵ and thickness δ_m, strong hydrophobicity must prevent membrane wetting through large pores.

5. Concluding remarks

The molar flux of water vapor across the membrane pore was analytically derived using temperatures at membrane interfaces. Our fundamental theory agrees reasonably well with experimental observation of the vapor flux reported in the literature. The ideal gas law was used to relate the local partial pressure and number concentration of water vapor. An alternative representation of vapor pressure of saturated water was derived using an

empirical equation of latent heat, which is a linearly decreasing function of temperature. Mean free path and Brownian diffusivity were calculated as a function of molar fractions of water vapor and air, and found to be very gradually decreasing with respect to temperature. The effective diffusion coefficient is calculated using the Bosanquet relationship; and as expected, the membrane pore diameter primarily determines the dominance of Knudsen flow over Brownian diffusion. The temperature profile is proven to be exponentially changing along the membrane pore, but the dominance of heat conduction through the solid membrane makes the temperature profile axially monotonous. More importantly, the constant pressure assumption (experimentally verified) implies that the total concentration increases from the pore inlet to the outlet, which indirectly supports that the prediction of the effective diffusivity and the mean free path decrease as the temperature decreases along the pore. The heat flux is (almost) linearly proportional to the vapor flux, and its variance with respect to the flux is very small. Given an overall temperature difference between the feed and the permeate, i.e., T_1-T_4, a higher feed temperature (or a higher permeate temperature) provides higher flux, which primarily stems from the non-linearity of the water vapor pressure (equivalently vapor concentration calculated using the idea gas law) with respect to temperature. A broad pore size distribution always decreases the vapor flux as compared to that of mono-dispersed distribution, because the log-normal distribution switches the peak location to the left of the mean value, providing more small pores.

Acknowledgments

This research was supported by Kyung Hee University International Scholar Program, and the corresponding author would like to specially thank Prof. Weilin Qu with University of Hawaii for illuminating discussions.

Appendix A

This section includes detailed derivations and implications of basic thermodynamic quantities closely related to DCMD processes.

A.1. Mass transfer across the membrane

A.1.1. Clausius-Clapeyron equation and molar latent heat of water

The basic representation of the Clausius–Clapeyron equation at the liquid–gas (i.e., water–vapor) equilibrium is

$$\frac{dp}{dT}=\frac{\Delta S}{\Delta \mathcal{V}} \tag{A.1}$$

where ΔS and $\Delta \mathcal{V}$ are changes in molar entropy and volume associated with the phase transformation between the two phases. The transformation takes place at the constant temperature T, and the entropy change is simply

$$\Delta S=\frac{l(T)}{T} \tag{A.2}$$

where $l(T)$ is the latent heat of the liquid, and T is the temperature of the phase transformation. Because the gas phase has a much bigger molar volume, $\mathcal{V}_g$, than that of the water phase $\mathcal{V}_w$, one can assume that the change in molar volume is approximately equal to the gas phase molar volume: $\Delta \mathcal{V}=\mathcal{V}_g-\mathcal{V}_w\approx \mathcal{V}_g$. In addition, the ideal gas law can be applied to characterize the vapor thermodynamic state in the membrane pore: $p\mathcal{V}=RT$, where R is the universal gas constant. The general representation of the Clausius–Clapeyron equation along the phase transformation line between pressure and temperature is then

$$\frac{1}{p}\frac{dp}{dT}=\frac{l(T)}{RT^2} \tag{A.3}$$

which indicates two important issues in describing the DCMD process. (See Appendix A.1.1 for details.) First, the Clausius–Clapeyron equation should be separately applied at the pore inlet of T_2 and outlet of T_3 because it underlies a constant temperature for the phase transformation. The mean temperature $\overline{T}$, roughly estimated as $\frac{1}{2}(T_2+T_3)$ or $\frac{1}{2}(T_1+T_4)$, can be used to estimate dP/dT quantitatively, but its physical meaning is questionable because no phase transformation between water and vapor occurs at $\overline{T}$. Second, the temperature dependence of the latent heat $l(T)$ must be carefully studied and included to describe DCMD transport phenomena for accurate quantitative analysis of the vapor pressure, p. In this work, we developed an alternative experimental correlation of water vapor pressure related to water latent heat. (See Appendix A.1.2 for details.)

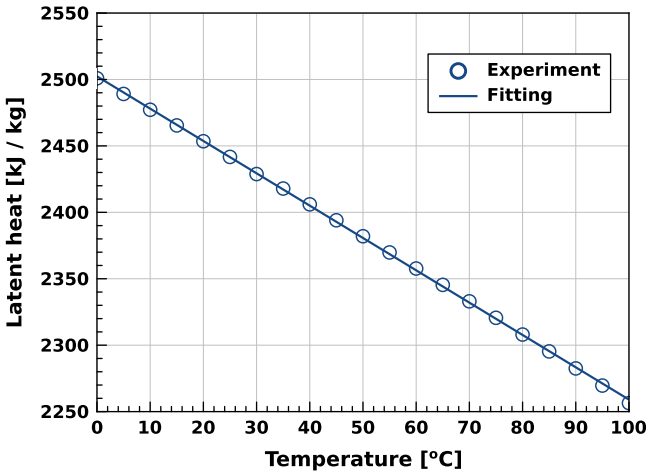

Fig. A1. Latent heat (enthalpy) of liquid water per mass versus temperature, i.e., the heat needed to be adsorbed for water evaporation at a given temperature T. The solid line is obtained from the linear regression using Eq. (A.4). Data are from Ref. [23].

A.1.2. Latent heat of saturated water: data fitting

Fig. A1 shows the variation of the latent heat of saturated water with respect to temperatures ranging from 0 °C to 100 °C. Data used are obtained from Ref. [23] and our linear regression gives

$$l(T)=l_0-l_1T \tag{A.4}$$

where T is the absolute temperature, and l_0 and l_1 are calculated using linear regression. Using water of density 10^3 kg/l and molar concentration 55.49 mol/l, we obtained $l_0=57.075$ kJ/mol and $l_1=4.3856\times10^{-2}$ kJ/mol K. Water density changes only 2.8% from 10 °C to 80 °C and therefore l_0 and l_1 must be indifferent to the operating temperatures of the DCMD process. Substitution of Eq. (A.4) into (A.3) and solving Eq. (A.3) for pressure p gives

$$p(T)=p_0\exp\left(-\frac{L(T)}{RT}\right) \tag{A.5}$$

and its derivative with respect to temperature

$$\frac{dp}{dT}=p_0\left(\frac{l_0-l_1T}{RT^2}\right)e^{-L(T)/RT} \tag{A.6}$$

where

$$L(T)=l_0+l_1T\ln T \tag{A.7}$$

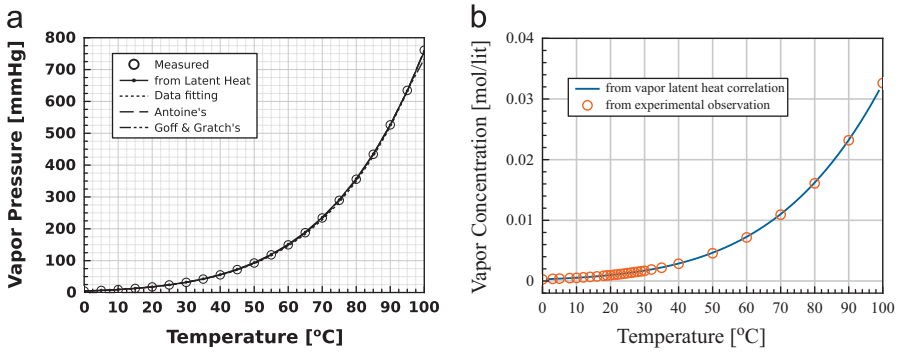

Fig. A2. Variation of (a) water vapor pressure and (b) concentration versus temperature. The vapor pressure representation (of Eq. (A.8)) derived from the water latent heat profile has a good agreement with the measured data obtained from Ref. [23]. Fitting Eq. (A.9), Antoine's Eq. (A.10), and Goff-Gratch Eq. (A.11) (of Ref. [24]) also provide equal accuracy.

and $p_0 = 2.71690 \times 10^{24}$ mmHg (with standard error of 0.09381%) is an integration constant of pressure determined by comparing Eq. (A.5) with experimental data. Note that Eq. (A.5) can be used as the partial pressure of water vapor in the membrane pore as a function of the local membrane temperature, and Eq. (A.6) indicates that the gradient of the partial pressure (equivalent to the concentration gradient) controls the vapor flux through the membrane pore. The Clausius–Clapeyron equation (in terms of dp/dT) inserted in Eq. (9) emphasizes that phase transformation equilibria are separately maintained at the feed–membrane and membrane–permeate interfaces of different temperatures.

A.1.3. Vapor pressure and concentration

In this section, we discuss empirical correlations of vapor pressure and estimated vapor concentration, as shown in Fig. A2, with respect to temperature as listed below.

1. We rewrite Eq. (A.5) in the following form:

$$p = p_0 T^{-l_1/R} \exp\left[-\frac{l_0/R}{T}\right] = T^{-l_1/R} \exp\left[\ln p_0 - \frac{l_0/R}{T}\right] \tag{A.8}$$

   Note that the constant terms of l_0 and l_1 of the latent heat Eq. (A.4) generate in Eq. (A.8) the exponential and power-wise dependences on temperature, respectively.

2. Vapor pressure data of water can be directly fitted to provide

$$p_{\text{fit}}\ (\text{mmHg}) = \exp\left(a - \frac{b}{T}\right) \tag{A.9}$$

   where $a = 20.386$ and $b = 5132$ K. Although this equation can be a good functional approximation, its mathematical form implicitly assumes that the latent heat of the saturated water is independent of temperature. In other words, coefficients a and b of Eq. (A.9) can be obtained by setting $l_1 = 0$ of the latent heat and calculating a different set of l_0 and p_0 in Eq. (A.8). Therefore, although Eq. (A.9) provides quantitatively accurate values, the functional form does not include intrinsic physical consistency.

3. Antoine's equation is expressed as

$$\log_{10}(p_{\text{Ant}}\ (\text{mmHg})) = A - \frac{B}{C - 273.15 + T} \tag{A.10}$$

   where $A = 8.07131$, $B = 1730.63$ K, and $C = 233.426$ K. A series expansion of the right hand of Eq. (A.10) can generate an empirical function that corresponds to $T^{-l_1/R}$ of Eq. (A.8), but the Taylor series does not provide a closed-form expression.

4. As stated in the previous section, the water vapor pressure is the upper limit of the partial pressure of water in the membrane pore. Conventionally, the maximum partial pressure of water vapor in air phase was estimated using the Goff–Gratch equation [24]

$$\begin{aligned}\log_{10}\left(\frac{p\ (\text{mmHg})}{1.3332239}\right) = {} & -7.90298\left(\frac{373.16}{T} - 1\right) \\ & + 5.02808 \log_{10}\left(\frac{373.16}{T}\right) \\ & - 1.3716 \times 10^{-7}\left(10^{11.344(1 - T/373.16)} - 1\right) \\ & + 8.1328 \times 10^{-3}\left(10^{-3.49149(373.16/T - 1)} - 1\right) \\ & + \log_{10}(1013.246)\end{aligned} \tag{A.11}$$

For engineering purposes, selection of the vapor pressure expressions among Eqs. (A.8)–(A.10) is arbitrary but with specific mathematical convenience; and use of the partial pressure of Eq. (A.11) is conceptually more rigorous in engineering science although its numerical accuracy needs to be checked.

Fig. A2(a) shows that the above four semi-empirical pressure representations of water vapor in air are in good agreement with experimental measurements. However, use of Eq. (A.8) provides a better fundamental understanding between the vapor pressure and the latent heat of saturated water: $l_0 - l_1 T_0$ implies the molar latent heat is at the freezing point of water, and l_1 indicates the declining rate of the latent heat with respect to the absolute temperature. It is worth noting that the use of Eqs. (A.8)–(A.10) presumes that a thermodynamic equilibrium is maintained at (both) the inlet and outlet of the membrane pore, which was erroneously approximated using the mean temperature. Fig. A2(b) shows the vapor concentration profile with respect to temperature. The ideal gas law was used to calculate molar concentration of water vapor, and water vapor pressure was calculated using Eq. (A.8). Calculated vapor concentration shows a similar non-linear behavior to that of the vapor pressure, which starts near 40–50 °C. This is because the vapor concentration is proportional to p/T and temperature ranges from 273.5 K to 373.5 K.

A.1.4. Mean free path

Mass transfer mechanisms of water vapor through the membrane pores can be classified into three models: molecular (Brownian) diffusion, Knudsen diffusion, and viscous (Poiseullie) flow. Lawson and Lloyd [7] reported that the viscous flow has a negligible impact on the mass transport of DCMD processes (see next section for details). This observation implies that the total pressure in the membrane pore is almost a constant, and

counter-interdiffusion of water vapor and air governs primarily the performance of DCMD process, i.e., $n_T = n_a + n_w = \text{const.}$

The relative significance between the Brownian and Knudsen diffusion mechanisms can be determined using the standard Knudsen number (Kn), defined as

$$\text{Kn} = \frac{\lambda}{d_p} \tag{A.12}$$

where λ is the mean free path of molecules, interpreted as the mean distance traveled by a molecule between consecutive collisions with other molecules. Flow regimes in the pore spaces can be specifically categorized as: (1) $\text{Kn} < 10^{-3}$ for continuum flow, (2) $10^{-3} < \text{Kn} < 10^{-1}$ for slip flow on the solid-liquid interface, (3) $10^{-1} < \text{Kn} < 10$ for transition flow, and (4) $10 < \text{Kn}$ for free molecular flow.

Detailed discussion on the flow regime and the Knudsen diffusion influenced by pore geometry can be found elsewhere [17]. For a single component gas, the mean free path is inversely proportional to the molecular number concentration n:

$$\lambda = \frac{1}{\sqrt{2} n \sigma_0} \tag{A.13}$$

where $\sigma (= \pi d_c^2)$ is the scattering cross section and d_c is the collision diameter of traveling molecules.

If water vapor collides with only neighboring water vapor such that the gas phase consists of only water vapor (of 100% humidity) at total pressure P_T, then Eq. (A.13) can be interpreted by replacing n by P_T/k_BT as

$$\lambda = \frac{k_B T}{\sqrt{2} P_T \sigma_{ww}} \tag{A.14}$$

where $\sigma_{ww} (= \pi d_w^2)$ is the scattering cross sectional area between two water molecules of collision diameter $d_w = 2.641 \times 10^{-10}$ m.

Since the DCMD performance is primarily governed by vapor transport from the feed–membrane to membrane–permeate interfaces, the gas phase needs to be considered as a binary mixture consisting of water vapor and air molecules. Ref. [21] used the following expression to estimate the mean free path of water vapor:

$$\lambda_{w-a} = \frac{k_B T}{\pi ((d_w + d_a)/2)^2 P_T} \frac{1}{\sqrt{1 + m_w/m_a}} \tag{A.15}$$

where $d_a = 3.711 \times 10^{-10}$ m is the air collision diameter. The fundamental meaning of Eq. (A.15) should be carefully investigated as follows. Due to the partial pressure of water vapor being lower than that of air, water vapor collides with air molecules only, and these collision events are characterized by the mutual collision diameter, $\frac{1}{2}(d_w + d_a)$, and molecular weight ratio of m_w/m_a. At 60 °C, $\lambda_{w-a} = 0.1$ μm was estimated using Eq. (A.15). Due to this implicit physical restriction of Eq. (A.15), λ_{w-a} should be calculated only if the water vapor concentration is negligible compared to the air concentration. The ratio of collision diameters of air to water, $d_a/d_w = 1.4053$, and that of their molecular weights, $m_a/m_w = 1.60174$, do not significantly deviate from unity so that Eq. (A.15) can be an approximation to calculate an order of magnitude of the mean free path in the membrane pore. If the membrane pore is, however, filled with water vapor only, then λ_{w-w} can be calculated by arbitrarily setting $d_a \to d_w$ and $m_a \to m_w$. Perhaps an experimental setup of an initial low vacuum phase in the DCMD module, followed by natural water evaporation at the feed–membrane interface, can mimic this theoretical limit.

In general, the mean free path of water vapor must be fundamentally expressed as follows:

$$\lambda_w = \frac{\overline{v}_w}{\overline{V}_{ww} n_w \sigma_{ww} + \overline{V}_{wa} n_a \sigma_{wa}} = \frac{\overline{v}_w}{n_T (\overline{V}_{ww} x_w \sigma_{ww} + \overline{V}_{wa} x_a \sigma_{wa})} \tag{A.16}$$

where $\overline{v}_w$ is the mean speed of water vapor, $\overline{V}_{ww}$ and $\overline{V}_{wa}$ are the relative mean speed of water vapor to targeting water vapor and an air molecule, respectively; n_w and n_a are the concentrations of water vapor and air molecules, respectively, and $n_T = n_w + n_a$ is the total concentration in the gas phase; and $\sigma_{ww} = \pi d_w^2$ and $\sigma_{wa} = \pi (d_w + d_a)^2/4$ are collision diameters between two water vapor molecules and water vapor and air molecules, respectively.

For vapor–vapor and vapor–air collisions, the relative mean speeds can be approximated as

$$V_{ww} \simeq \sqrt{\langle v_w^2 \rangle + \langle v_w^2 \rangle} = \sqrt{2 \langle v_w^2 \rangle} \simeq \overline{v}_w \sqrt{2} \tag{A.17}$$

$$V_{wa} \simeq \sqrt{\langle v_w^2 \rangle + \langle v_a^2 \rangle} = \sqrt{\langle v_w^2 \rangle} \sqrt{1 + m_w/m_a} \simeq \overline{v}_w \sqrt{1 + m_w/m_a} \tag{A.18}$$

where the mean speed is assumed to be close to the root-mean-square speed: $\overline{v}_w \simeq \sqrt{\langle v_w^2 \rangle}$. This is because each water and air molecule has the same kinetic energy so that $\frac{1}{2} k_B T = \frac{1}{2} m_w \langle v_w^2 \rangle = \frac{1}{2} m_a \langle v_a^2 \rangle$. Then, Eq. (A.16) can be re-organized as

$$\lambda_w = \frac{k_B T}{\sigma_{ww} P_w \sqrt{2} + \sigma_{wa} P_a \sqrt{1 + m_w/m_a}} \tag{A.19}$$

in terms of the partial pressures and temperature instead of the total concentration. λ_w in Eq. (A.19) varies with partial pressures of water vapor and air molecules, and λ_{w-a} in Eq. (A.15) becomes accurate as the water partial (vapor) pressure is much smaller than 1 atm.

Fig. A3 shows the mean free paths of water vapor in the gas phase within the membrane pore. The top dotted line assumes that the gas phase has 100% humidity so that molecular collisions are only between water vapor molecules. As noted above, water vapor and air molecules have effective collision diameters of $d_w = 2.641 \times 10^{-10}$ m and $d_a = 3.711 \times 10^{-10}$ m, respectively. Therefore, the cross section for vapor–vapor collisions is smaller than that of vapor–air collisions. The dashed line assumes a very low water vapor concentration, meaning that collisions of water

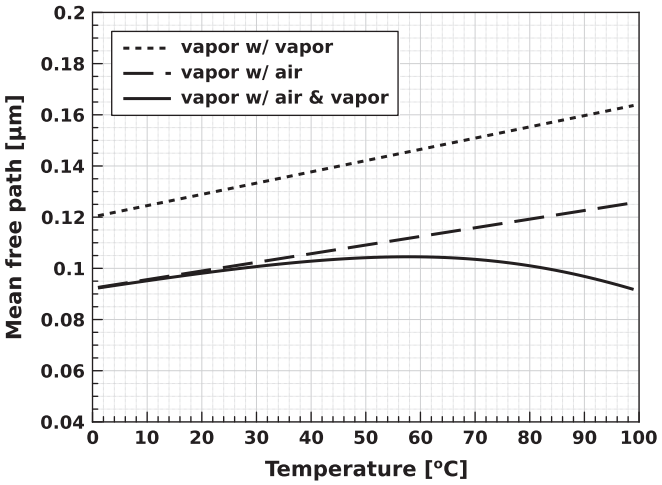

Fig. A3. Estimation of mean free path of water vapor. The dotted and dashed lines indicate that water molecules collide with other water vapor molecules (Eq. (A.14)) or air molecules (Eq. (A.15)) only, respectively; and the solid line represents the effect of water vapor fraction in the gas phase on its mean free path using Eq. (A.19). Decreasing temperature from feed to permeate interfaces is equivalent to increasing axial distance z from 0 to δ_m as indicated in Eq. (6).

vapor molecules are mostly with air molecules of larger diameter. In this case, the mean free path is shorter than that of vapor–vapor collisions. The total pore pressure must not be lower than the initial pore pressure due to water evaporation at the feed–membrane interface and is assumed to be 1.0 atm for simplicity. The solid line uses the total pressure in the membrane pore as the initial air pressure of 1 atm , $P_T = P_{atm}$, which indicates that the mean free path of water vapor does not significantly vary with respect to the feed temperature even if the large temperature difference is applied across the membrane. The high temperature T_2 produces water vapor of high kinetic energy at the pore inlet, increases fractional concentration of water vapor, and increases the total pressure from the initial state. Water vapor molecules of higher energy move faster, but encounter more collisions per unit time. As a consequence, the mean free path of water vapor molecules is a pseudo-constant (≈ 0.1 μm) due to the counter effects of molecular energy and concentration with respect to temperature.

In the previous section, the Knudsen number was introduced as a ratio of the mean free path to the pore diameter. In statistical physics, the Brownian diffusivity is determined as the mean of squared displacements between two collisions divided by the mean collision time. This can be approximated as the product of the mean molecular speed and mean free path. On the other hand, the Knudsen diffusivity is proportional to the pore size multiplied by the mean molecular speed. To determine the dominant diffusion mechanism, a ratio of Brownian to Knudsen diffusivity can be an alternative choice of the Knudsen number

$$\mathrm{Kn} = \frac{\lambda}{d_p} \rightarrow \frac{D_B}{D_K} \propto T^{1.572}$$

Note that the standard form of the Stokes–Einstein diffusion coefficient ($k_B T/3\pi\mu d_c$, where μ is the medium viscosity) does not hold for Brownian diffusion of water vapor in the gaseous binary mixture in terms of dependency on T. True dependence of the Knudsen number on the ambient temperature needs rigorous investigation at the molecular level, which is out of the research scope of this paper. However, the dominance of the diffusion mechanism may not change significantly along the membrane pore because the temperature difference between the feed and permeate does not usually exceed 40–50 °C. As shown in Fig. A3, λ ranges from 0.09 to 0.12 μm as temperature varies from 0 °C to 100 °C. Typical pore sizes of DCMD membranes are of an order of magnitude of $O(10^{-1})$ μm, which is only a few factors larger than the mean free path. In this case, the Knudsen number must reside between 0.1 and 10 so tat the mass flow is in the transition region where the Knudsen and Brownian diffusion compete with each other and therefore the effective diffusivity of Eq. (10) needs to be introduced.

A.1.5. Flux estimation using mean temperature

The permeate flux J_w is estimated using the mean temperature $\overline{T}$ across the membrane. Equating Eqs. (9) and (13) gives

$$C_m = \frac{D_e(\overline{T})}{\delta_m k_B \overline{T}} \tag{A.20}$$

Then, Eq. (9) is fully written as

$$\bar{J}_w = \frac{D_e(\overline{T})}{\delta_m k_B \overline{T}} \left[\frac{dp}{dT}\right]_{T=\overline{T}} (T_2 - T_3) \tag{A.21}$$

where dp/dT is calculated using Eq. (A.6). For the mean temperature approximation, $\bar{J}_w$ was used for the iteration process written in Section 3.1.2.

A.2. Heat transfer across the membrane

A.2.1. Local balance

A set of differential governing equations (instead of Eqs. (1)–(3)) for heat flux, Q_m, across the membrane of porosity ϵ may be expressed in terms of water–vapor (w), air (a), and solid (s) contributions

$$q_w = -\overline{k}_w \frac{dT}{dz} + H_w J_w \tag{A.22}$$

$$q_a = -\overline{k}_a \frac{dT}{dz} + H_a J_a \tag{A.23}$$

$$q_s = -\overline{k}_s \frac{dT}{dz} \tag{A.24}$$

where $\overline{k}_w = k_w x_w \epsilon$, $\overline{k}_a = k_a(1-x_w)\epsilon$, and $\overline{k}_s = k_s(1-\epsilon)$. In Eqs. (A.22)–(A.24), k_i is the thermal conductivity, x_i is the molar fraction satisfying $x_a + x_w = 1$, and H_i and J_i are the molar enthalpy and flux, respectively. We assumed that the interdiffusion between water vapor and air occurs in opposite directions to each other; and the molar flux ratio is inversely proportional to their molecular weight ratio:

$$J_a = -\beta J_w \tag{A.25}$$

where $\beta = \sqrt{m_w/m_a}$: using molecular weights of water and air, $m_w = 18.05$ g/mol and $m_a = 28.97$ g/mol [23], respectively, one calculates $\beta = 0.788575$.

Because heat fluxes of water vapor and air (q_w and q_a, respectively) occur due to the common driving force of the temperature gradient dT/dz and individual inter-diffusive fluxes (J_w and J_a), the net heat flux in the gas-phase (q_g) is: $q_g = q_w + q_q$. This superposition is equivalent to an electric circuit with two resistances in parallel because the additive molar flux corresponds to the electric current. The equivalent resistance must be $(\overline{k}_w + \overline{k}_a)^{-1}$, and therefore the net heat conductivity in the pore spaces is equal to $\overline{k}_w + \overline{k}_a$. Then, the gas phase heat flux due to the vapor–air interdiffusion can be expressed as

$$q_g = q_w + q_a = -(\overline{k}_w + \overline{k}_a)\frac{dT}{dz} + \overline{H} J_w \tag{A.26}$$

where

$$\overline{H} = H_w - \beta H_a \tag{A.27}$$

is the effective molar enthalpy of the vapor–air mixture in the membrane pore.

As the heat transfer across the membrane is geometrically divided into parallel solid and void parts of the membrane, q_g and q_s should be added in the same manner. The total heat flux across the membrane is then

$$Q_m = q_g + q_s = -\overline{k}\frac{dT}{dz} + \overline{H} J_w \tag{A.28}$$

where $\overline{k}$ is the effective heat conductivity of the porous membrane expressed as

$$\overline{k} = \overline{k}_w + \overline{k}_a + \overline{k}_s \tag{A.29}$$

Specific values of the thermal conductivities of air and water vapor can be found elsewhere [5,23], and that of membrane materials usually range $k_s = 0.1$–0.3 W/m K.

A.2.2. Effective molar enthalpy

The partial molar enthalpy of air is

$$H_a = c_{p,a} T \tag{A.30}$$

and evaporation enthalpy of water–vapor at temperature T is

$$H_w = l(T_0) + c_{p,w} \times (T - T_0) \tag{A.31}$$

where $c_{p,a}$ and $c_{p,w}$ are the heat capacity of air and water at constant pressure, respectively, and $l(T_0)$ is the latent heat of saturated water at the freezing temperature T_0=273.15 K. The effective molar enthalpy of Eq. (A.27) is re-written as

$$\overline{H} = \overline{H}_0 - \overline{c}_p T \tag{A.32}$$

where $\overline{H}_0 = l(T_0) - c_{pw}T_0$ and $\overline{c}_p = c_{pw} - \beta c_{pa}$.

A.2.3. Effective thermal conductivity

Estimation of the effective heat conductivity $\overline{k}$ of Eq. (A.29) requires information about k_w, k_a, and k_s which can be taken from the literature or reference data. The membrane porosity ϵ can be provided by membrane vendors or calculated using microscopic image processing of the membrane surface. The molar fraction of water vapor x_w must be calculated as a fraction of the partial pressure of water vapor at temperature $T(z)$ in equilibrium with the (internal) membrane pore surfaces. The axial variation of the molar fraction can represent the effective thermal conductivity as a function of z. However, due to mathematical complexity, we use the mean molar fraction of water vapor to calculate $\overline{k}$. This approximation is sound because the thermal conductivity of the (solid) membrane (k_s) is usually one order of magnitude higher than that of air and vapor and, more importantly, independent of mole fractions. The pseudo-constant molar fractions of air and vapor are represented as

$$x_a = \frac{P_a}{P_T} \tag{A.33}$$

and

$$x_w = \frac{P_w}{P_T} \tag{A.34}$$

where P_T is the total pressure inside the membrane pore, and P_a and P_w are the partial pressures of air and vapor, respectively.

A.2.4. Temperature profile along the membrane pore

Substitution of the molar enthalpy $\overline{H}$ of Eq. (A.27) into the heat flux Eq. (A.28) gives

$$Q = -\overline{k}\frac{dT}{dz} + (\overline{H}_0 - \overline{c}_p T)J_w \tag{A.35}$$

The heat flux Q and molecular vapor flux J_w are independent of the axial coordinate z in the steady state. We define dimensionless variables for temperature and distance, $\tau = T/T_0$ and $Z = z/\delta_m$

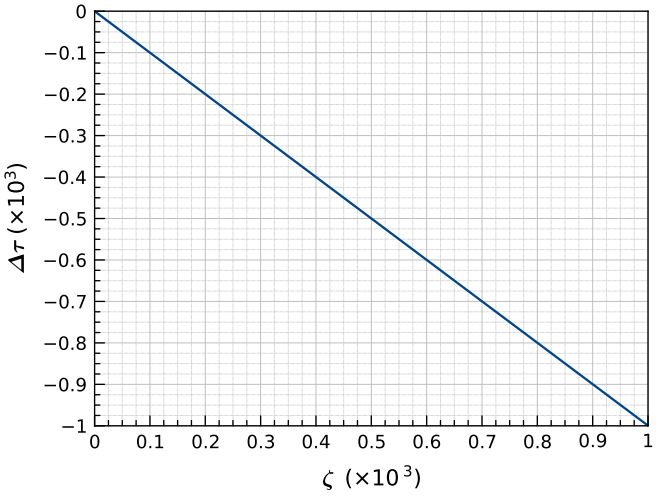

Fig. A4. Profile of the dimensionless temperature difference $\Delta\tau$ versus dimensionless distance ζ of Eq. (A.37).

and rewrite the above heat flux Eq. (A.35) as

$$\frac{d\tau}{dZ} = -(a + b\tau) \tag{A.36}$$

where $a = (Q - J_w\overline{H}_0)/(\overline{k}T_0/\delta_m)$ and $b = J_w\overline{c}_pT_0/(\overline{k}T_0/\delta_m)$. Integration of Eq. (A.36) and applying the inlet boundary condition $\tau(Z=0) = T_2/T_0$ provides

$$\Delta\tau = e^{-\zeta} - 1 \tag{A.37}$$

where

$$\Delta\tau = \frac{T(z) - T_2}{T_2 + \dfrac{q - J_w\overline{H}_0}{J_w\overline{c}_p}} \tag{A.38}$$

and

$$\zeta = \frac{J_w\overline{c}_p z}{\overline{k}} \tag{A.39}$$

are dimensionless temperature difference and axial distance from the pore inlet, respectively. Fig. A4 shows the linear variation of $\Delta\tau$ with respect to ζ. Eq. (A.37) indicates that the temperature decreases exponentially along the membrane pore, but the small membrane thickness and large conductivity $\overline{k}$ make the temperature profile linearly decrease with respect to ζ: $\Delta\tau = e^{-\zeta} - 1 \approx (1-\zeta) - 1 = -\zeta$. Because of the small range of ζ, the $\Delta\tau$ profile is consistently monotonous even near its maximum: $\zeta \to J_w\overline{c}_p\delta_m/\overline{k}$. Then, the rigorous temperature profile is solved as

$$T(z) = T_2 - \left(T_2 + \frac{Q - J_w\overline{H}_0}{J_w\overline{c}_p}\right)(1 - e^{-J_w\overline{c}_p z/\overline{k}}) \tag{A.40}$$

and the membrane heat flux Q is calculated by applying the boundary condition at the pore outlet, $T(z=\delta_m) = T_3$

$$Q = (T_2 - T_3)\left(\frac{J_w\overline{c}_p}{1 - e^{-J_w\overline{c}_p\delta_m/\overline{k}}}\right) + J_w(\overline{H}_0 - \overline{c}_pT_2) \tag{A.41}$$

which replaces Eq. (2). Note that Eq. (A.41) represents the DCMD heat flux in terms of interfacial temperatures T_2 and T_3. Specific heat capacity values of feed and permeate, h_f and h_p, respectively, can determine the interfacial temperatures using the bulk temperatures of T_1 and T_4 [25].

Physical quantities in the exponential term of Eq. (A.41) have the following ranges or orders of magnitude: molar vapor flux $J_w = O(0.1)$ mol/m^2 s [7,21], effective thermal conductivity $\overline{k} \approx \frac{1}{2}k_s$ because the membrane porosity has typical values of $\epsilon = 0.6-0.8$ [2,5,7] and molar fraction of water vapor and air are between 0 and 1; and the effective heat capacity at constant pressure is calculated as $\overline{c}_p = 53.0412$ J/mol K. Here we estimate

$$\frac{J_w\overline{c}_p\delta_m}{\overline{k}} \sim \frac{0.1 \times 53 \times 10^{-4}}{0.1} = O(10^{-3}) \tag{A.42}$$

which indicates that the heat transport through the membrane pore of length δ_m due to interdiffusion of water vapor and air molecules with the effective heat capacity $\overline{c}_p$ is much smaller than the conductive heat flux through the solid membrane material, i.e., $J_w\overline{c}_p\delta_m \ll \overline{k}$, by at least two orders of magnitude.

Nomenclature *Symbols*

C_m	mass transfer coefficient through the membrane pore (mol/m^2 s Pa)
$c_{p,w}$	heat capacity of water at constant pressure (kJ/kg K)
$c_{p,a}$	heat capacity of air at constant pressure (kJ/kg K)
D_B	Brownian diffusivity (m^2/s)
d_c	collision diameter (m)
D_e	effective diffusivity (m^2/s)

D_K	Knudsen diffusivity (m^2/s)
d_p	pore diameter (m)
H_a	molar enthalpy of air (kJ/mol)
h_m	(effective) heat transfer coefficient across the membrane (W/m^2 K)
H_w	molar enthalpy of water vaporization (kJ/mol)
J_a	molar flux of air through membrane pore (mol/m^2 s)
J_p	permeate flux of water vapor (mol/m^2 s)
J_w	molar flux of water vapor through membrane pore (mol/m^2 s)
k_a	thermal conductivity of air (0.026 W/m K)
k_m	thermal conductivity of membrane (W/m K)
k_w	thermal conductivity of water (0.020 W/m K)
$l(T)$	latent heat of liquid water as a function of temperature T (kJ/mol)
m_a	molecular weight of air, 28.97 g/mol
m_w	molecular weight of water, 18.05 g/mol
$n(z)$	axial number concentration (#/m^3)
n_a	number concentration of air (#/m^3)
n_T	total number concentration (#/m^3)
n_w	number concentration of water vapor [#/m^3]
p,p_w	vapor pressure of water (Pa)
P_a	partial pressure of air (Pa)
p_a	initial gas phase pressure in the membrane pore (1.0 atm)
P_T	total pressure (in the membrane pore) (Pa)
P_w	partial pressure of water vapor (Pa)
Q	heat flux (W/m^2)
q	heat flux across the membrane (W/m^2)
S	structural number (–)
T	temperature (K)
T_0	freezing temperature of water, 0 °C or 273.15 K
t_m	membrane tortuosity
x_a	molar fraction of air
x_w	molar fraction of water
Kn	Knudsen number

Greek letters

β	square root of molar mass ratio of water to air, $\sqrt{m_w/m_a}$
$\Delta\mathcal{V}$	molar volume change for phase transformation (m^3/mol)
δ_m	membrane thickness (m)
ΔS	molar entropy change for phase transformation (J/K)
ΔT_m	temperature difference between membrane interfaces (K)
λ	mean free path (m)
$\mathcal{V}$	molar volume
σ	collision cross section (m^2)
τ	dimensionless temperature
ζ	dimensionless ditance with thermal parameters

Subscripts

c	collision
e	effective
f	feed
g	gas phase
m	porous membrane
p	permeate
s	solid part of membrane
1	bulk feed
2	feed–membrane interface
3	membrane–permeate interface
4	bulk permeate

Mathematical symbols

$\overline{H}$	effective molar enthalpy (kJ/mol)
$\overline{k}$	effective thermal conductivity (W/m K)
$\overline{T}$	mean temperature (K)
$\overline{V}$	mean relative speed (m/s)
$\overline{v}$	mean molecular speed (m/s)

References

[1] Marcel Mulder, Basic Principles of Membrane Technology, 2nd ed., Kluwer Academic Publishers, 1996.
[2] Mohamed Khayet, T Matsuura, Membrane Distillation: Principles and Applications, Elsevier, 2011.
[3] Efrem Curcio, Enrico Drioli, Membrane distillation and related operations—a review, Sep. Purif. Rev. 34 (1) (2005) 35–86.
[4] A.M. Alklaibi, Noam Lior, Membrane-distillation desalination: status and potential, Desalination 171 (2) (2005) 111–131.
[5] Mohamed Khayet, Membranes and theoretical modeling of membrane distillation: a review, Adv. Colloid Interface Sci. 164 (1–2) (2011) 56–88.
[6] Abdullah Alkhudhiri, Naif Darwish, Nidal Hilal, Membrane distillation: a comprehensive review, Desalination 287 (2028) (2012).
[7] Kevin W. Lawson, Douglas R. Lloyd, Membrane distillation. II. Direct contact MD, J. Membr. Sci. 120 (1) (1996) 123–133.
[8] A.M. Alklaibi, Noam Lior, Transport analysis of air-gap membrane distillation, J. Membr. Sci. 255 (1–2) (2005) 239–253.
[9] C.H. Bosanquet, British TA Rept., 1944, pp. BR–507.
[10] M. Gryta, M. Tomaszewska, A.W. Morawski, Membrane distillation with laminar flow, Sep. Purif. Technol. 11 (2) (1997) 93–101.
[11] L. Martinez-Diez, M.I. Vazquez-Gonzalez, Temperature and concentration polarization in membrane distillation of aqueous salt solutions, J. Membr. Sci. 156 (2) (1999) 265–273.
[12] R.W. Schofield, A.G. Fane, C.J.D. Fell, Heat and mass transfer in membrane distillation, J. Membr. Sci. 33 (3) (1987) 299–313.
[13] Fortunato Lagana, Giuseppe Barbieri, Enrico Drioli, Direct contact membrane distillation: modelling and concentration experiments, J. Membr. Sci. 166 (1) (2000) 1–11.
[14] Mohamed Khayet, Armando Velázquez, Juan I. Mengual, Modelling mass transport through a porous partition: effect of pore size distribution, J. Non Equilib. Thermodyn. 29 (3) (2004) 279–299.
[15] Martin Knudsen, Willard Fisher, The molecular and the frictional flow of gases in tubes, Phys. Rev. Ser. I 31 (5) (1910) 586–588.
[16] J.C. Maxwell, Treatise on Electricity and Magnetism, Dover, New York, 1881.
[17] Yong Shi, Yong Lee, Albert S. Kim, Knudsen Diffusion Through Cylindrical Tubes of Varying Radii: Theory and Monte Carlo Simulations, Transport in Porous Media, Online Now, 2012, pp. 1–25.
[18] Albert S. Kim, H. Chen, Diffusive tortuosity factor of solid and soft cake layers: a random walk simulation approach, J. Membr. Sci. 279 (1–2) (2006) 129–139.
[19] T.R. Marrero, E.A. Mason, Gaseous diffusion coefficients, J. Phys. Chem. Ref. Data 1 (1) (1972) 3–118.
[20] Anthony F. Mills, Mass Transfer, 2nd ed., Prentice Hall, New Jersey, 2001.
[21] J. Phattaranawik, R. Jiraratananon, A.G. Fane, Effect of pore size distribution and air flux on mass transport in direct contact membrane distillation, J. Membr. Sci. 215 (1–2) (2003) 75–85.
[22] Jason Woods, John Pellegrino, Jay Burch, Generalized guidance for considering pore-size distribution in membrane distillation, J. Membr. Sci. 368 (1–2) (2011) 124–133.
[23] Yunus A. Cengel, Michael A. Boles, Thermodynamics, An Engineering Approach, 7th ed., New York, NY, 2011.
[24] J.A. Goff, S. Gratch, Low-pressure properties of water from −160 to 212 F, in: Transactions of the American Society of Heating and Ventilating Engineers, the 52nd Annual Meeting of the American Society of Heating and Ventilating Engineers, 1946, pp. 95–122.
[25] J. Phattaranawik, R. Jiraratananon, A.G. Fane, Heat transport and membrane distillation coefficients in direct contact membrane distillation, J. Membr. Sci. 212 (1–2) (2003) 177–193.